



OPEN

Deep learning supports the differentiation of alcoholic and other-than-alcoholic cirrhosis based on MRI

Julian A. Luetkens^{1,7}, Sebastian Nowak^{1,7}, Narine Mesropyan¹, Wolfgang Block^{1,2,3}, Michael Praktijnjo⁴, Johannes Chang⁴, Christian Bauckhage^{5,6}, Rafet Sifa⁶, Alois Martin Sprinkart^{1,7}✉, Anton Faron^{1,7} & Ulrike Attenberger^{1,7}

Although CT and MRI are standard procedures in cirrhosis diagnosis, differentiation of etiology based on imaging is not established. This proof-of-concept study explores the potential of deep learning (DL) to support imaging-based differentiation of the etiology of liver cirrhosis. This retrospective, monocentric study included 465 patients with confirmed diagnosis of (a) alcoholic (n = 221) and (b) other-than-alcoholic (n = 244) cirrhosis. Standard T2-weighted single-slice images at the caudate lobe level were randomly split for training with fivefold cross-validation (85%) and testing (15%), balanced for (a) and (b). After automated upstream liver segmentation, two different ImageNet pre-trained convolutional neural network (CNN) architectures (ResNet50, DenseNet121) were evaluated for classification of alcohol-related versus non-alcohol-related cirrhosis. The highest classification performance on test data was observed for ResNet50 with unfrozen pre-trained parameters, yielding an area under the receiver operating characteristic curve of 0.82 (95% confidence interval (CI) 0.71–0.91) and an accuracy of 0.75 (95% CI 0.64–0.85). An ensemble of both models did not lead to significant improvement in classification performance. This proof-of-principle study shows that deep-learning classifiers have the potential to aid in discriminating liver cirrhosis etiology based on standard MRI.

As the end stage of chronic liver disease, liver cirrhosis is a major health issue. In particular, patients with liver cirrhosis have a concomitant risk for the development of hepatocellular carcinoma as well as complications arising from decompensation such as variceal bleeding or hepatic encephalopathy. Overall, the prevalence of chronic liver disease is internationally expected to grow within the next decades^{1–3}.

Many factors that contribute to the development of cirrhosis have been identified. The most common etiologies are alcohol consumption, obesity, and chronic viral infections³. Thereby, identification of the underlying cause of disease is crucial as appropriate treatment may not only stop disease from progression, but in certain cases also may facilitate regression of fibrosis^{2,4,5}. In the majority of countries, alcohol consumption still represents the leading cause of liver disease and is directly related to liver mortality^{3,6}. In these patients, alcohol abstinence was shown to be critical for long-term outcome, may improve various aspects of disease severity and is also fundamental with regard to potential liver transplantation^{4,7,8}. However, until experiencing severe complications such as acute decompensation, many patients with cirrhosis are unaware of their underlying condition^{2,3}. Liver cirrhosis results from chronic inflammation and hence leads to distinct changes in hepatic morphology, which in part can be detected by high-resolution imaging methods such as MRI^{9,10}.

¹Department of Diagnostic and Interventional Radiology, Quantitative Imaging Lab Bonn (QILaB), University Hospital Bonn, Venusberg-Campus 1, 53127 Bonn, Germany. ²Department of Radiotherapy and Radiation Oncology, University Hospital Bonn, Venusberg-Campus 1, 53127 Bonn, Germany. ³Department of Neuroradiology, University Hospital Bonn, Venusberg-Campus 1, 53127 Bonn, Germany. ⁴Department of Internal Medicine I, Center for Cirrhosis and Portal Hypertension Bonn (CCB), University Hospital Bonn, Venusberg-Campus 1, 53127 Bonn, Germany. ⁵Institute for Computer Science, University of Bonn, Endenicher Allee 19C, 53113 Bonn, Germany. ⁶Media Engineering Department, Fraunhofer IAIS, Schloss Birlinghoven 1, 53757 Sankt Augustin, Germany. ⁷These authors contributed equally: Julian A. Luetkens, Sebastian Nowak, Alois Martin Sprinkart, Anton Faron and Ulrike Attenberger. ✉email: Sprinkart@uni-bonn.de

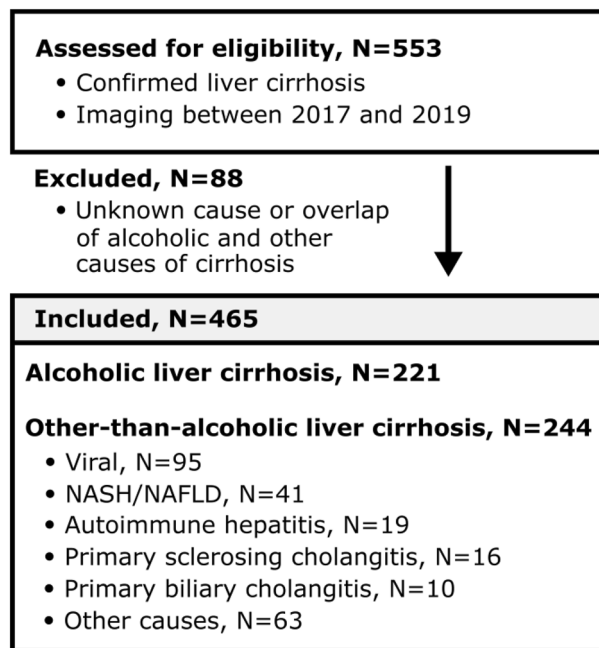


Figure 1. Study inclusion flow chart. Patients with confirmed diagnosis of liver cirrhosis who underwent liver MRI between 2017 and 2019 were evaluated for inclusion. Patients with unknown causes of liver cirrhosis and with documented overlap of alcoholic liver cirrhosis with other causes were excluded from the analysis. The final cohort consisted of 465 patients. Those patients were separated according to liver cirrhosis etiology into patients with (a) alcoholic liver cirrhosis (N = 221) and (b) other-than-alcoholic liver cirrhosis (N = 244). Abbreviations: NAFLD/NASH non-alcoholic fatty liver disease/non-alcoholic steatohepatitis.

Although it has been described that the micro- and macroscopic appearance of cirrhosis in medical imaging varies to some extent according to the underlying etiology, the use of imaging features as a means to determine the cause of the disease has not been established yet^{9,11,12}. In a previous study, a convolutional neural network (CNN) was already shown to be able to detect liver cirrhosis based on standard clinical MRI sequences with expert-level accuracy irrespective of etiology¹³. Therefore, the aim of this proof-of-concept study was to investigate deep learning for standard MRI based characterization of disease etiology, differentiating alcoholic- versus other-than-alcoholic cirrhosis.

Materials and methods

Dataset. The study was approved by the Ethics Committee at the Medical Faculty of the Rheinische Friedrich-Wilhelms-Universität Bonn and the need for written informed consent was waived due to its retrospective, single-center nature. The research was performed in accordance with the Declaration of Helsinki. Patients with confirmed diagnosis of liver cirrhosis, defined by clinical manifestations of liver cirrhosis (e.g. presence of dermal features, ascites, splenomegaly or hyperestrogenism), laboratory parameters (e.g. presence of parameters of hepatocyte damage or impaired hepatic synthesis), and/or histopathological criteria, who underwent liver MRI for diagnostic purposes between 2017 and 2019 at the Department of Diagnostic and Interventional Radiology at the University Hospital of Bonn, were evaluated for inclusion. The clinical information management system of the relevant institution was used to derive clinical characteristics of the study population including the respective cause of liver cirrhosis. Patients with unknown causes of liver cirrhosis and with overlap of alcoholic and other causes were excluded. The final cohort was separated according to the underlying cause of liver cirrhosis into (a) patients with alcoholic liver cirrhosis and (b) other-than-alcoholic liver cirrhosis (Fig. 1).

Image segmentation and classification. All patients underwent a standardized imaging protocol including a standard clinical respiratory triggered multi-slice turbo spin echo sequence with non-cartesian k-space filling (T2 MultiVane XD) on a clinical 1.5 Tesla (Ingenia 1.5 T, Philips Healthcare, Best, the Netherlands) or 3.0 Tesla (Ingenia 3.0 T, Philips Healthcare, Best, the Netherlands) scanner. This sequence was shown to be suitable for deep learning-based detection of liver cirrhosis in a previous study¹³. Similar to the proposed approach for cirrhosis detection, a single cross-sectional image at the level of caudate lobe was exported, followed by liver segmentation performed by a U-net style convolutional neural network (CNN) with ResNet34 as backbone that was developed and validated on a dataset of 713 single slice T2- weighted MRI images¹³. The images were first normalized and image augmentation was applied during training. Supplementary information on imaging parameters and image preprocessing can be found in Supplement S1 and S2.

For imaging development of a classification CNN that differentiates patients with alcoholic liver cirrhosis and other-than-alcoholic liver cirrhosis, data were randomly split into a training (85%) and a hold-out test set

(15%). Training was performed with fivefold cross-validation. An ensemble of the cross-validated models was applied to the test set.

A CNN with residual connections (ResNet50) with ImageNet pre-trained parameters was used, as this established architecture was shown to be suitable for the detection of liver cirrhosis^{13,14}. To investigate whether the use of a different pre-trained architecture than ResNet50 or an ensemble of two architectures is beneficial, a CNN with dense connections (DenseNet121) was additionally evaluated, which has fewer trainable parameters and is less computationally intensive compared to ResNet50¹⁵.

Furthermore, two different training strategies were evaluated for ResNet50 and DenseNet121 in order to examine whether altering the pre-trained parameters of the CNN may impact classification performance. First, both networks were trained with frozen pre-trained parameters of the convolutional layers. In a second subsequent training run, the pre-trained convolutional layers of both networks were unfrozen with descending learning rates from the last to the first layer at several stages. Training was performed with Adam optimization, a cyclical learning rate scheme, and cross-entropy loss function. Supplementary information on the experimental design and hyper-parameters used for training are provided in Supplement S3.

Image regions that were particularly relevant to the classification task were highlighted by generating gradient-weighted class activation maps (Grad-CAM) for the test set¹⁶.

Statistical analysis. Prism 8 (GraphPad software), SPSS Statistics 24 (IBM), MedCalc 20.014 (MedCalc Software Ltd) and Scikit-learn 0.23.2¹⁷ were used for statistical analysis. Patient characteristics are expressed as frequencies or means with standard deviation, as appropriate. Classification accuracy (ACC), as well as receiver operating characteristic (ROC) analyses was performed for the cross-validation and the test sets for both studied CNN architectures (ResNet50, DenseNet121) and both training strategies (frozen, unfrozen). For the test set, 95% confidence intervals were determined for ACC and AUC values. ROC and precision-recall curves were generated¹⁸. Grad-CAM images were visually inspected by one experienced radiologist (A.F.) and highlighted regions were categorized according to their anatomical localization as being predominantly situated in the right liver lobe, the left liver lobe, the portal region, the caudate lobe, or in the image background. Resulting categorical data were compared using either Fisher's exact test (for a cell count of ≤ 5) or χ^2 test (for a cell count > 5), as appropriate. The two-sided t-Test was used to compare differences between groups regarding continuous variables. $P < 0.05$ was set as the level of statistical significance.

Results

Baseline characteristics of the study population. A total of 465 patients (203 female; mean age, 60 ± 11 years) were included. Of those, 47.5% (221/465) of patients had alcoholic liver cirrhosis. 52.5% (244/465) of patients had other-than-alcoholic liver cirrhosis.

Liver biopsy was performed in 64.8% (301/465) of patients. The most common causes of non-alcohol related liver cirrhosis were viral hepatitis (39%, 95/244), non-alcoholic fatty liver disease or non-alcoholic steatohepatitis (17%, 41/244), and autoimmune hepatitis (8%, 19/244). In 5% (12/244) of patients with other-than-alcoholic liver cirrhosis, etiology of liver disease was multifactorial. Causes of liver cirrhosis of the entire study population are summarized in detail by Table 1. No significant differences regarding age (61 ± 9 years vs. 59 ± 13 years, $P = 0.110$) and gender distribution (48%, 105/221 female patients vs. 40%, 98/244 female patients, $P = 0.111$) were observed between patients with alcoholic and other-than-alcoholic liver cirrhosis. There was no difference in weight between patients with alcoholic and other-than-alcoholic cirrhosis (80.1 ± 20.4 kg vs. 80.1 ± 17.7 kg, $P = 0.972$). Values for γ -glutamyltransferase were higher in patients with alcoholic cirrhosis compared to patients with other-than-alcoholic cirrhosis (208.8 ± 264.1 U/l vs. 147.4 ± 166.1 U/l, $P = 0.003$).

Classification of liver cirrhosis etiology. Segmented images of the entire study population were randomly subdivided into a training (N = 396; 174 female; mean age, 60 ± 12 years), and a test set (N = 69; 29 female; mean age, 59 ± 10 years), with training sets being further split for fivefold cross-validation, balanced for patients with alcoholic and non-alcoholic cause of liver cirrhosis.

Trained with frozen parameters, a mean accuracy (ACC) and mean area under the curve (AUC) of 0.69 and 0.78 was observed for ResNet50 and a mean ACC of 0.66 and a mean AUC of 0.78 was observed for DenseNet121 for all 5 validation splits (Table 2). With unfrozen pre-trained parameters, mean ACC values of 0.74 and 0.71 and mean AUC values of 0.83 and 0.82 were obtained for ResNet50 and DenseNet121 on cross-validated training data, respectively.

On test data, the classification performance of ResNet50 was higher than DenseNet121 when training with unfrozen parameters, however the difference was not statistically significant (Value and 95% CI: $AUC_{ResNet50}$ 0.82 [0.71–0.91] vs. $AUC_{DenseNet121}$ 0.79 [0.67–0.88], $P = 0.40$; $ACC_{ResNet50}$ 0.75 [0.64–0.85] vs. $ACC_{DenseNet121}$ 0.70 [0.57–0.80], $P = 0.26$). Also, training with unfrozen parameters did not differ significantly compared to frozen parameters for both ResNet50 and DenseNet121 ($AUC_{ResNet50}$ 0.82 [0.71–0.91] vs. 0.82 [0.71–0.90], $P = 0.91$; $ACC_{ResNet50}$ 0.75 [0.64–0.85] vs. 0.74 [0.62–0.84], $P = 0.78$; $AUC_{DenseNet121}$ 0.79 [0.67–0.88] vs. 0.80 [0.69–0.89], $P = 0.69$; $ACC_{DenseNet121}$ 0.70 [0.57–0.80] vs. 0.74 [0.62–0.84], $P = 0.43$).

The ensemble of the two architectures did not lead to statistically significant improvement on the test set compared to ResNet50, neither for frozen ($AUC_{Ensemble}$ 0.84 [0.73–0.92] vs. $AUC_{ResNet50}$ 0.82 [0.71–0.90], $P = 0.54$; $ACC_{Ensemble}$ 0.75 [0.64–0.85] vs. $ACC_{ResNet50}$ 0.74 [0.62–0.84], $P = 0.78$), nor for unfrozen ($AUC_{Ensemble}$ 0.81 [0.70–0.90] vs. $AUC_{ResNet50}$ 0.82 [0.71–0.91], $P = 0.70$; $ACC_{Ensemble}$ 0.71 [0.59–0.81], vs. $ACC_{ResNet50}$ 0.75 [0.64–0.85], $P = 0.40$) pre-trained parameters.

ROC and precision-recall curves of the models trained with unfrozen pre-trained parameters are given in Fig. 2.

Etiology of liver cirrhosis	Number of patients (%)
Alcoholic liver cirrhosis	221 (48%)
Other-than-alcoholic liver cirrhosis	244 (52%)
Hepatitis B virus	26 (6%)
Hepatitis C virus	69 (15%)
Fatty liver disease (NAFLD/NASH)	41 (9%)
Autoimmune hepatitis	19 (4%)
Primary sclerosing cholangitis	16 (3%)
Drug-induced	13 (3%)
Primary biliary cholangitis	10 (2%)
Portal vein thrombosis	9 (2%)
Nutritional	9 (2%)
Budd-Chiari syndrome	9 (2%)
Hemochromatosis	5 (1%)
Idiopathic	5 (1%)
Sinusoidal obstruction syndrome	3 (1%)
Secondary sclerosing cholangitis	3 (1%)
Alpha-1 Antitrypsin Deficiency	3 (1%)
Wilson disease	2 (< 1%)
Congestive hepatopathy	1 (< 1%)
Sarcoidosis	1 (< 1%)

Table 1. Liver cirrhosis etiology. Underlying causes of liver cirrhosis are reported for the entire study population (N = 465) as total numbers as well as percentages of the entire study cohort. *NAFLD/NASH* non-alcoholic fatty liver disease/non-alcoholic steatohepatitis.

	Frozen pre-trained parameters						Unfrozen pre-trained parameters					
	ResNet50		DenseNet121		Ensemble		ResNet50		DenseNet121		Ensemble	
	AUC	ACC	AUC	ACC	AUC	ACC	AUC	ACC	AUC	ACC	AUC	ACC
Training + validation												
Split 1	0.737	0.684	0.764	0.671	0.776	0.658	0.798	0.696	0.780	0.671	0.807	0.709
Split 2	0.774	0.658	0.751	0.646	0.768	0.747	0.773	0.722	0.839	0.684	0.798	0.684
Split 3	0.800	0.722	0.797	0.646	0.815	0.722	0.864	0.785	0.817	0.772	0.876	0.797
Split 4	0.821	0.709	0.822	0.658	0.852	0.684	0.879	0.785	0.858	0.722	0.870	0.759
Split 5	0.742	0.671	0.756	0.684	0.770	0.722	0.822	0.722	0.805	0.696	0.813	0.709
Mean	0.775	0.689	0.778	0.661	0.796	0.707	0.827	0.742	0.820	0.709	0.833	0.732
Test												
	0.819	0.739	0.801	0.739	0.838	0.754	0.823	0.754	0.786	0.696	0.813	0.710

Table 2. Classification performance of the cross-validation and testing of the CNN architectures trained with frozen and unfrozen pre-trained parameters. Classification accuracy and AUC values for each validation split of the cross-validation and mean over all splits. The classification accuracy and AUC values of ensembles of the cross-validated models on the test set. *AUC* area under the curve, *ACC* accuracy.

Highlighted imaging regions according to Grad-CAM. The decision process to classify liver cirrhosis as being alcohol related or non-alcohol related was further visualized using Grad-CAM analysis for ResNet50 trained with unfrozen pre-trained parameters. According to Grad-CAM analysis, the right liver lobe (alcoholic liver cirrhosis 42%, 14/33; other-than-alcoholic liver cirrhosis 61%, 22/36) and the portal area (alcoholic liver cirrhosis 30%, 10/33; other-than-alcoholic liver cirrhosis 19%, 7/36) were the imaging regions that were most frequently decisive for the classification process in both groups. Thereby, no significant differences regarding distribution of decisive imaging regions between the two patient groups were observed (Table 3). Exemplary images of the Grad-CAM analysis are provided in Fig. 3.

Discussion

The purpose of this study was to investigate whether a deep learning-based analysis can aid in differentiating the etiology of liver cirrhosis based on routine clinical T2-weighted MRI. Acceptable to excellent discriminatory ability was found in distinguishing patients with alcoholic and other-than-alcoholic cirrhosis. In a previous

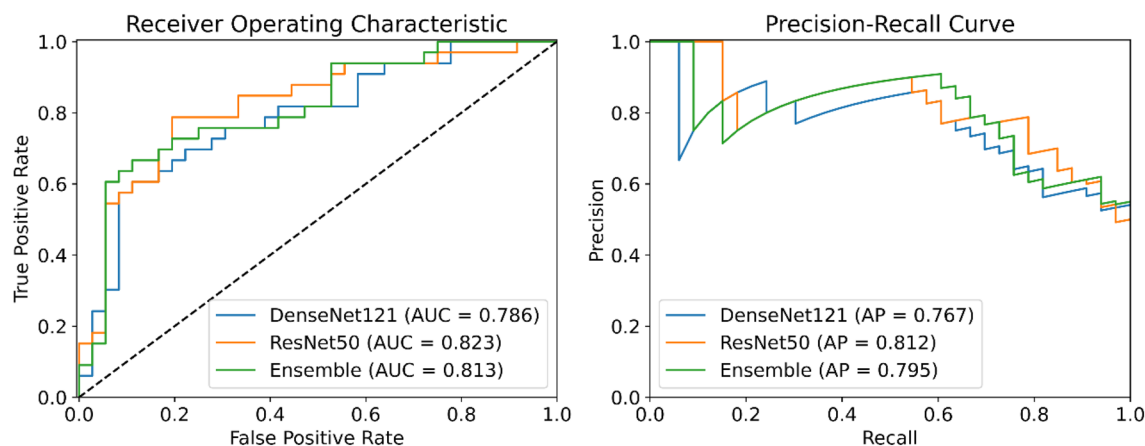


Figure 2. Receiver operating characteristic and precision-recall analysis for the classification performance of DenseNet121 and ResNet50, both trained with unfrozen pre-trained parameters. Abbreviations: *AUC* area under the curve, *AP* average precision.

	Alcoholic liver cirrhosis (N = 33)	Other-than-alcoholic liver cirrhosis (N = 36)	P value
Right lobe	14 (42%)	22 (61%)	0.12
Left lobe	3 (9%)	3 (8%)	1.00
Portal area	10 (30%)	7 (19%)	0.30
Caudate lobe	4 (12%)	1 (3%)	0.19
background	2 (6%)	3 (8%)	1.00

Table 3. Highlighted imaging regions according to gradient-weighted class activation maps (Grad-CAM). Results of the visual inspection of Grad-CAM images classified by ResNet50 are provided. Within each segmented image of the test set, highlighted regions were visually rated as being primarily located within the right liver lobe, the left liver lobe, the portal area, the caudate lobe, or within image background by one radiologist experienced in abdominal imaging (A.F.).

study, a ResNet50 with frozen pre-trained ImageNet parameters was proposed for automatic detection of liver cirrhosis on T2-weighted MRI¹³. The results of our proof-of-concept study extend the findings of this previous report and show that deep learning not only enables the detection of cirrhosis, but can also help in identifying the underlying cause of the disease.

Although the ability of the ImageNet pre-trained ResNet50 to discriminate between alcoholic and other-than-alcoholic cirrhosis can be described as excellent¹⁹, it is inferior to the differentiation of cirrhotic versus non-cirrhotic livers¹³. This may be due to less distinctiveness between imaging criteria indicating different causes of the disease compared to image criteria distinguishing a diseased organ from a non-diseased organ. For instance, it has been described that a hypertrophic appearance of the central hepatic parenchyma/caudate lobe is expected in alcohol-related cirrhosis, but also in primary sclerosing cholangitis and Budd-Chiari syndrome related cirrhosis¹¹.

Of both models investigated in the current study, ResNet50 showed higher classification performance on test data. However, the performance was not significantly higher compared to Densenet121. Interestingly, for both CNNs, subsequent training with unfrozen pre-trained parameters did not significantly increase classification performance on test data. This may suggest that the extraction capabilities of general imaging features of the convolutional kernels, learned during the pre-training with the ImageNet database, generalize well to T2-weighted MRI images. An ensemble of the two models trained with unfrozen parameters achieved equal accuracy and a slightly higher AUC compared to ResNet50, however, the difference was not statistically significant. Therefore, no clear advantage was observed by using an ensemble of the two different pre-trained ImageNet architectures.

Grad-CAM-analysis indicate that the imaging morphology of the right liver lobe and caudate lobe seem to comprise particularly relevant information for discrimination of alcoholic from other-than-alcoholic liver cirrhosis. This is in line with previous studies, which describe that the right posterior hepatic notch sign, defined as a sharp liver surface indentation at the posterior boundary of the right and caudate lobe, is considered to be particularly prevalent among patients with alcoholic liver cirrhosis^{12,20}. As described above, hypertrophies of the caudate lobe and central hepatic areas are more frequently observed in patients with alcohol-related diseases, but are also seen in other etiologies. To the best of our knowledge, there are currently no studies presenting metrics for the diagnostic accuracy of cirrhosis etiology based on such imaging criteria^{11,12}. However, a very recent work investigated a radiomics approach that relates imaging features to the etiology of liver cirrhosis, and also achieved promising results²¹. Unlike the deep learning method presented in the current study, the proposed radiomics approach requires manual definition of region of interests. To date, imaging features have not been used in routine clinical practice to identify alcohol as a cause of cirrhosis.

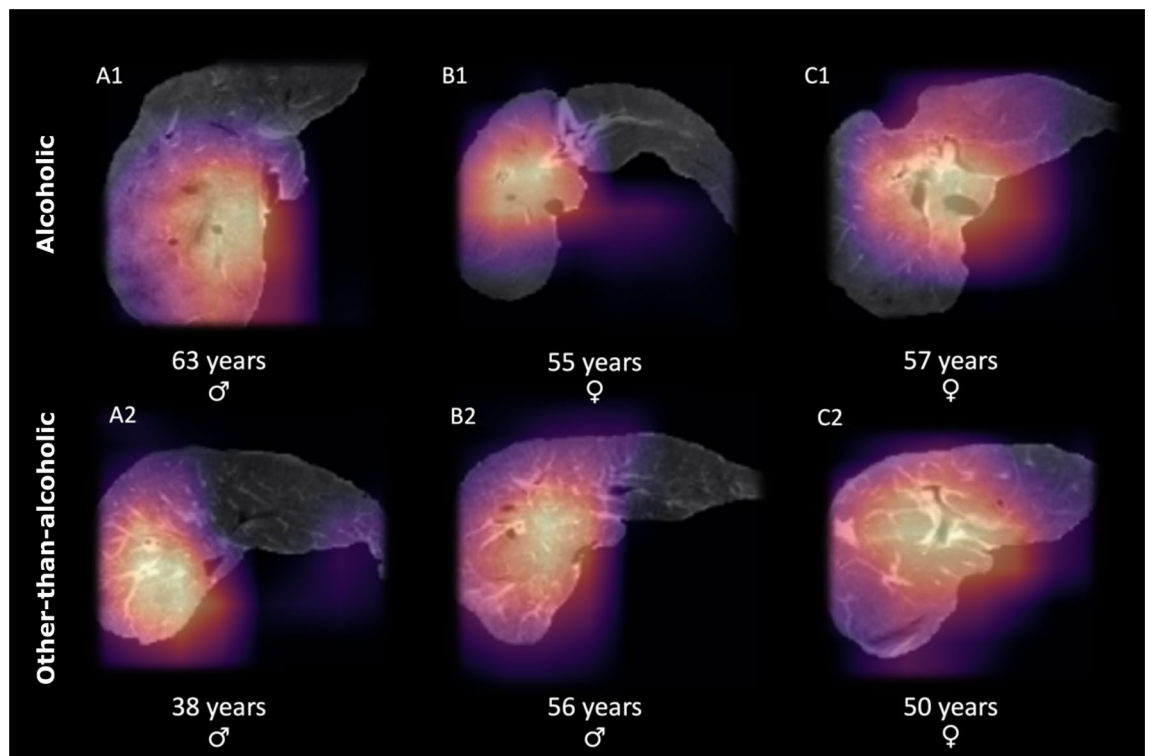


Figure 3. Exemplary images from the study population. ResNet50 trained with unfrozen pre-trained parameters was used for the classification task. Exemplary patients from the test set are provided and imaging regions that were particularly relevant to the classification task are highlighted using the gradient-weighted class activation maps (Grad-CAM) method. Panels A1, B1, C1 provide exemplary patients from the test set with alcoholic liver cirrhosis. In panels A2, B2, C2, images of exemplary patients from the test set with other-than-alcoholic liver cirrhosis are presented. In panels A1, B1, A2, B2, regions within the right liver lobe appeared to be particularly relevant for the classification task, as indicated by Grad-CAM images. In panels C1 and C2, the portal liver region appeared to be most decisive for classification.

In clinical routine, liver cirrhosis is typically diagnosed by a combination of characteristic clinical and imaging findings, corresponding laboratory testing and ancillary examinations such as abdominal sonography. Thereby, while this work-up is usually straightforward for virus-related cirrhosis, it may be much more effortful in patients with alcohol-related disease, which in many cases may be diagnosed only by exclusion since there are no specific laboratory findings²². Liver biopsy is recommended if cirrhosis etiology is uncertain, but is limited due to its invasive nature, inter-observer variability and potential sampling error^{2,23}. Moreover, cirrhosis-related parenchymal changes may hamper or even preclude correct histological analysis².

Compensated liver cirrhosis is frequently asymptomatic; thus, it may be assumed that many patients who undergo routine clinical MRI for other indications may be unaware of a concomitant liver disease. In these patients, a pipeline that automatically identifies tissue alterations and can classify possible disease etiologies has the potential to better guide diagnostic pathways and thus initiate a specific therapy earlier. With the help of deep learning algorithms simple cross-sectional imaging modalities could serve as imaging-based biomarkers for the classification of liver disease in the future. Particularly in alcoholic liver cirrhosis, timely and correct identification of the underlying etiology is crucial, as early abstinence was demonstrated to be the key determinant of long-term outcome^{8,24}. Sole clinical assessment of alcoholic liver disease alone might not be trivial in clinical practice because it mostly relies on patients' self-report. In this regard, deep learning applications have the potential to aid diagnosis by extracting also relevant information that may not be readily apparent to the human eye.

Our study has several limitations. The algorithm was developed for binary classification only and does currently not support differentiation of various non-alcohol-related cirrhosis etiologies. Due to the limited number of patients within the respective subclasses and to ensure collectives of comparable size for classification, we decided to pool patients with other-than-alcoholic cirrhosis. Future studies with larger samples of the respective subgroups are needed to substantiate the findings from this proof-of-concept study and to expand its application. The clinical benefit would also be significantly increased by an extension to other etiologies. Especially, NAFLD is becoming the main cause of chronic liver disease in many countries and the detection of metabolic related cirrhosis on cross-sectional imaging should be further explored in future studies. Also, we were not able to analyze possible coexisting etiologies of liver cirrhosis in our explorative analysis, as detailed data on additional risk factors were not available due to the retrospective study design. However, future studies should evaluate the ability of deep learning methods to differentiate overlapping liver disease, such as both alcoholic and non-alcoholic steatohepatitis (BASH). Moreover, we exclusively used single-slice T2-weighted images of segmented livers and ImageNet pre-trained models, as these have been shown to be suitable for the detection of liver cirrhosis in a

previous study¹³. Future studies may also address a three-dimensional approach accounting also for extrahepatic manifestations in cirrhotic patients or the use of other imaging sequences for differentiation of etiologies.

In summary, the results of this proof-of-principle study demonstrate that discrimination between alcoholic and other-than-alcoholic cirrhosis based on clinical T2-weighted single-slice images is feasible with acceptable to excellent discrimination ability. This indicates the potential of deep learning for a more comprehensive assessment of diffuse liver disease.

Data availability

The data sets analysed in this study are subject to data protection law and are therefore not publicly available.

Received: 11 November 2021; Accepted: 9 May 2022

Published online: 18 May 2022

References

1. Kamath, P. S. Acute on chronic liver failure. *Clin. Liver Dis.* **9**(4), 86–88 (2017).
2. Wiegand, J. & Berg, T. The etiology, diagnosis and prevention of liver cirrhosis: Part 1 of a series on liver cirrhosis. *Dtsch. Arztebl. Int.* **110**(6), 85–91 (2013).
3. Pimpin, L. *et al.* Burden of liver disease in Europe: Epidemiology and analysis of risk factors to identify prevention policies. *J. Hepatol.* **69**(3), 718–735 (2018).
4. Huang, Y. W., Yang, S. S. & Kao, J. H. Pathogenesis and management of alcoholic liver cirrhosis: A review. *Hepat. Med.* **3**, 1–11 (2011).
5. Sohrabpour, A. A., Mohamadnejad, M. & Malekzadeh, R. Review article: The reversibility of cirrhosis. *Aliment. Pharmacol. Ther.* **36**(9), 824–832 (2012).
6. Terris, M. Epidemiology of cirrhosis of the liver: National mortality data. *Am. J. Public Health Nations Health.* **57**(12), 2076–2088 (1967).
7. Marroni, C. A. *et al.* Liver transplantation and alcoholic liver disease: History, controversies, and considerations. *World J. Gastroenterol.* **24**(26), 2785–2805 (2018).
8. Altamirano, J. *et al.* Alcohol abstinence in patients surviving an episode of alcoholic hepatitis: Prediction and impact on long-term survival. *Hepatology* **66**(6), 1842–1853 (2017).
9. Yeom, S. K., Lee, C. H., Cha, S. H. & Park, C. M. Prediction of liver cirrhosis, using diagnostic imaging tools. *World J. Hepatol.* **7**(17), 2069–2079 (2015).
10. Watanabe, A. *et al.* Magnetic resonance imaging of the cirrhotic liver: An update. *World J. Hepatol.* **7**(3), 468–487 (2015).
11. Schwoppe, R. B., Katz, M., Russell, T., Reiter, M. J. & Lisanti, C. J. The many faces of cirrhosis. *Abdom. Radiol.* **45**(10), 3065–3080 (2020).
12. Okazaki, H. *et al.* Discrimination of alcoholic from virus-induced cirrhosis on MR imaging. *Am. J. Roentgenol.* **175**(6), 1677–1681 (2000).
13. Nowak, S. *et al.* Detection of liver cirrhosis in standard T2-weighted MRI using deep transfer learning. *Eur. Radiol.* <https://doi.org/10.1007/s00330-021-07858-1> (2021).
14. He, K., Zhang, X., Ren, S. & Sun, J. Deep residual learning for image recognition. In *CVPR 2016*, 770–778 (2016).
15. Huang, G., Liu, Z., van der Maaten, L. & Weinberger, K. Q. Densely connected convolutional networks. In *CVPR 2017*, 4700–4708 (2017).
16. Selvaraju R. R. *et al.* Grad-CAM: Visual explanations from deep networks via gradient-based localization. In *CVPR 2017*, 618–626 (2017).
17. Pedregosa, F. *et al.* Scikit-learn: Machine learning in Python. *J. Mach. Learn. Res.* **12**, 2825–2830 (2011).
18. Saito, T. & Rehmsmeier, M. The precision-recall plot is more informative than the ROC plot when evaluating binary classifiers on imbalanced datasets. *PLoS ONE* **10**(3), e0118432 (2015).
19. Mandrekar, J. N. Receiver operating characteristic curve in diagnostic test assessment. *J. Thorac. Oncol.* **5**(9), 1315–1316 (2010).
20. Tan, K. C. The right posterior hepatic notch sign. *Radiology* **248**(1), 317–318 (2008).
21. Elkilany, A. *et al.* A radiomics-based model to classify the etiology of liver cirrhosis using gadoteric acid-enhanced MRI. *Sci. Rep.* **11**, 10778 (2021).
22. Sakhuja, P. Pathology of alcoholic liver disease, can it be differentiated from nonalcoholic steatohepatitis?. *World J. Gastroenterol.* **20**(44), 16474–16479 (2014).
23. Soresi, M., Giannitrapani, L., Cervello, M., Licata, A. & Montalto, G. Non invasive tools for the diagnosis of liver cirrhosis. *World J. Gastroenterol.* **20**(48), 18131–18150 (2014).
24. Verrill, C., Markham, H., Templeton, A., Carr, N. J. & Sheron, N. Alcohol-related cirrhosis: Early abstinence is a key factor in prognosis, even in the most severe cases. *Addiction* **104**(5), 768–774 (2009).

Author contributions

J.A.L., A.M.S.: study concept; S.N.: Programming of the Machine Learning application; N.M., M.P., J.C.: Workup of clinical cohort; S.N., A.F., A.M.S., C.B., R.S., J.A.L., U.A.: drafting the manuscript; W.B.: data management; A.F., S.N.: statistics; All authors reviewed the manuscript. J.L., S.N., A.M.S., A.F., and U.A. contributed equally.

Funding

Open Access funding enabled and organized by Projekt DEAL. A.F. was supported by a grant from the BONFOR research program (2020-2A-04). The funders had no influence on study conceptualization and design, collection and analysis of the data, manuscript preparation as well as the decision to publish.

Competing interests

The authors declare no competing interests.

Additional information

Supplementary Information The online version contains supplementary material available at <https://doi.org/10.1038/s41598-022-12410-2>.

Correspondence and requests for materials should be addressed to A.M.S.

Reprints and permissions information is available at www.nature.com/reprints.

Publisher's note Springer Nature remains neutral with regard to jurisdictional claims in published maps and institutional affiliations.



Open Access This article is licensed under a Creative Commons Attribution 4.0 International License, which permits use, sharing, adaptation, distribution and reproduction in any medium or format, as long as you give appropriate credit to the original author(s) and the source, provide a link to the Creative Commons licence, and indicate if changes were made. The images or other third party material in this article are included in the article's Creative Commons licence, unless indicated otherwise in a credit line to the material. If material is not included in the article's Creative Commons licence and your intended use is not permitted by statutory regulation or exceeds the permitted use, you will need to obtain permission directly from the copyright holder. To view a copy of this licence, visit <http://creativecommons.org/licenses/by/4.0/>.

© The Author(s) 2022